inorganics

MDPI

Article

A Mixed-Valence Tetra-Nuclear Nickel Dithiolene Complex: Synthesis, Crystal Structure, and the Lability of Its Nickel Sulfur Bonds

Mohsen Ahmadi, Jevy Correia, Nicolas Chrysochos and Carola Schulzke *

Institut für Biochemie, Universität Greifswald, Felix-Hausdorff-Straße 4, 17489 Greifswald, Germany; ahmadim.ug@gmail.com (M.A.); correiaj@uni-greifswald.de (J.C.); nc093759@uni-greifswald.de (N.C.)

* Correspondence: carola.schulzke@uni-greifswald.de; Tel.: +49-3834-420-4321

Received: 9 March 2020; Accepted: 3 April 2020; Published: 9 April 2020

Abstract: In this study, by employing a common synthetic protocol, an unusual and unexpected tetra-nuclear nickel dithiolene complex was obtained. The synthesis of the $[Ni_4(ecpdt)_6]^{2-}$ dianion (ecpdt = (*Z*)-3-ethoxy-3-oxo-1-phenylprop-1-ene-1,2-bis-thiolate) with two K^+ as counter ions was then intentionally reproduced. The formation of this specific complex is attributed to the distinct dithiolene precursor used and the combination with the then coordinated counter ion in the molecular solid-state structure, as determined by X-ray diffraction. $K_2[Ni_4(ecpdt)_6]$ was further characterized by ESI-MS, FT-IR, UV-Vis, and cyclic voltammetry. The tetra-nuclear complex was found to have an uncommon geometry arising from the combination of four nickel centers and six dithiolene ligands. In the center of the arrangement, suspiciously long Ni–S distances were found, suggesting that the tetrameric structure can be easily split into two identical dimeric fragments or two distinct groups of monomeric fragments, for instance, upon dissolving. A proposed variable magnetism in the solid-state and in solution due to the postulated dissociation was confirmed. The Ni–S bonds of the "inner" and "outer" nickel centers differed concurrently with their coordination geometries. This observation also correlates with the fact that the complex bears two anionic charges requiring the four nickel centers to be present in two distinct oxidation states (2 × +2 and 2 × +3), i.e., to be hetero-valent. The different coordination geometries observed, together with the magnetic investigation, allowed the square planar "outer" geometry to be assigned to d^8 centers, i.e., Ni^{2+}, while the Ni^{3+} centers (d^7) were in a square pyramidal geometry with longer Ni–S distances due to the increased number of donor atoms and interactions.

Keywords: mixed-valence complex; dithiolene ligand; tetra-nuclear nickel complex; X-ray structure; magnetic moment

1. Introduction

Ene-dithiolate or dithiolene ligands have been compounds of interest in the scientific community since the 1960s [1–5]. At first, they were mostly investigated for their complexes' electronic structures and reactivity, and then in the context of materials chemistry, e.g., regarding electronic and non-linear optical properties [6,7]. They have since also attracted much attention as model ligands for molybdopterin (mpt—a natural ligand found in the cofactors of molybdenum and tungsten-dependent oxidoreductases) [8–11]. A specific characteristic of dithiolene ligands is their non-innocence, i.e., their ability to donate electrons to the coordinated metal ion. Such behavior was also proposed and discussed for the molybdopterin ligand coordinated to molybdenum or tungsten concurrent with enzymatic turnover processes [12]. More recently, dithiolene ligands were employed in bioinorganic model chemistry targeting hydrogenase enzymes' active sites [13].

Nickel, as a bio-metal, is most often found in combination with sulfur donor atoms, including Ni–Fe hydrogenases, in which the nickel ion and the iron ion of the active site are bridged by cysteinate sulfur atoms. This has led to many related bio-inspired model compounds, including those in which two sulfur bridged nickel ions were used for such species [14–20].

From the very beginning of dithiolene chemistry, nickel has always been an integral part of many respective investigations, either in the course of the synthesis of dithiolene ligands [21,22] as a dithiolene ligand transmitter to other metal ions (e.g., molybdenum or tungsten) [21,23–27] or as a central metal of interest for potential applications [7,28–33]. Such applications of dithiolene-bearing compounds include molecular materials with conducting [34], magnetic [35,36], and optical [37] properties on account of their unique electronic structure.

A combination of sulfur donor dithiolene ligands and coordinated nickel ions is therefore relevant for problems related to bioinorganic and inorganic/materials chemistry and with respect to a focus on either ligands, metals, or both (i.e., their specific combination).

Homoleptic bis-dithiolene complexes, in particular those of group 10 and group 11 metals, $[M(dithiolene)_2]^{n-}$ (n = 0–2), most often exhibit a square planar geometry, which is occasionally slightly distorted [38–42]. Depending on the electron configuration, a tetrahedral geometry might also be accessible, for instance with Ag^+ [43]. Typically, when homoleptic nickel bis-dithiolene complexes oligomerize, sulfur donor atoms become bridging ligands occupying the apical position of one of the coordinated nickel centers in the square pyramidal geometry [31,44].

Metal dithiolene complexes are generally able to form different types of networks by covalent [45] and non-covalent bonds [46], while extended networks with nickel centers are comparatively rare. In cases where two or more nickel ions are bridged by dithiolene sulfur donor atoms, the metal centers might adopt different or partial formal oxidation states. These species can be stabilized by a significant contribution of the extended π-ligands to their frontier orbitals [35]. Respective observations were made with oligo-nuclear nickel complexes, such as $[Ni_2(edt)_3]^{2-}$, $[Ni_3(edt)_4]^{2-}$ (edt = ethane-1,2-di-thiolate) [47], $[Ni_2(dmit)_3]$ (*dmit* = 2-thione-1,3-dithiole-4,5-dithiolate) [48], $[AsPh_4]_2[Ni_3(pdt)_2(dmit)_2]$, and $[NEt_4]_2[Ni_5(edt)_4(dmit)_2]^{2-}$ (pdt = propane-1,2-dithiol, edt = ethane-1,2-dithiol, dmit = 2-thione-1,3-dithiole-4,5-dithiolate) [49]. In 2011, Neves et al. [35] reported an interesting mixed-valence tetra-nuclear nickel dithiolene complex $[K(18\text{-crown-}6)]_2[Ni_4(\alpha\text{-tpdt})_4]$ (α-tpdt = 2,3-thiophenedithiolate) with a structure that was unique at that time and constitutes the only known analog of the novel tetrameric complex which is presented here. The originally targeted nickel dithiolene complex in the present investigation was initially merely of interest as a dithiolene ligand transmitter to a molybdenum center in a procedure, which typically works rather well and is commonly applied in our group [21,23–25,50,51]. With the specific ligand system used (a dithiolene with one phenyl substituent on one carbon of the ene function and one carboxylic acid ethyl ester group on the other), the reaction did not turn out as expected. Instead of the envisaged mono-nuclear nickel bis-dithiolene complex, a mixed valence tetra-nuclear nickel complex was obtained, in which half of all dithiolene sulfur donor atoms were in bridging positions between the two nickel centers. As the obtained complex is a very uncommon type (only one precedent, [35]), nickel centers bridged to other cations (whether nickel or any other metal) by sulfur donor atoms are biologically relevant with regard to hydrogenases, and nickel dithiolene chemistry is generally important (as evidenced by significant ongoing publication activities—vide supra), the complex obtained was investigated comprehensively and in detail, and the results of this study are presented here.

2. Results and Discussion

One of the most reliable and comparatively convenient procedures for the synthesis of dithiolene ligands (originally developed by Garner's group in particular for those with unsymmetrical substitutions on the ene) employs the xanthogenation of α-bromoketones, followed by an acidic cyclization reaction [9,52]. Accordingly, the starting material in this study, ethyl benzoyl acetate, was treated with *N*-bromosuccinimide (NBS) in solvent-free conditions (Scheme 1) and purified by Kugelrohr distillation. The colorless oily product, **1**, was subsequently reacted with the potassium salt of *o*-isopropyl xanthate to replace

the bromine substituent by the R-CS_2^- moiety, affording xanthogenated compound **2** in 84% yield. The targeted dithiolene precursor 4-ethylcarboxylate-5-phenyl-1,3-dithiole-2-one (ecpdt = CO, **3**) was obtained as a colorless crystalline solid through an acidic cyclization reaction with H_2SO_4 in a diethyl ether/dichloromethane solvent system and purified by column chromatography. Ligand precursor **3** was characterized inter alia by single-crystal X-ray diffraction (Figure 1).

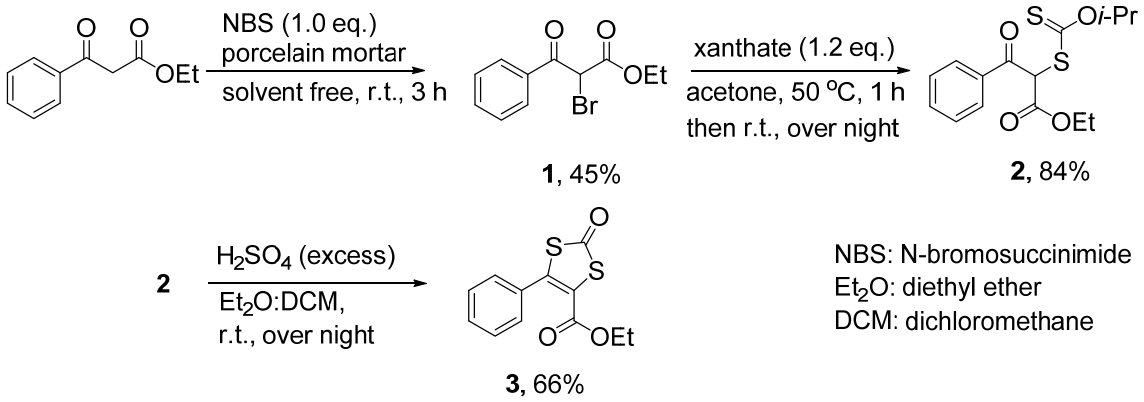

Scheme 1. The three-step preparation of ligand precursor ecpdt = CO (**3**) from commercially available ethyl benzoyl acetate.

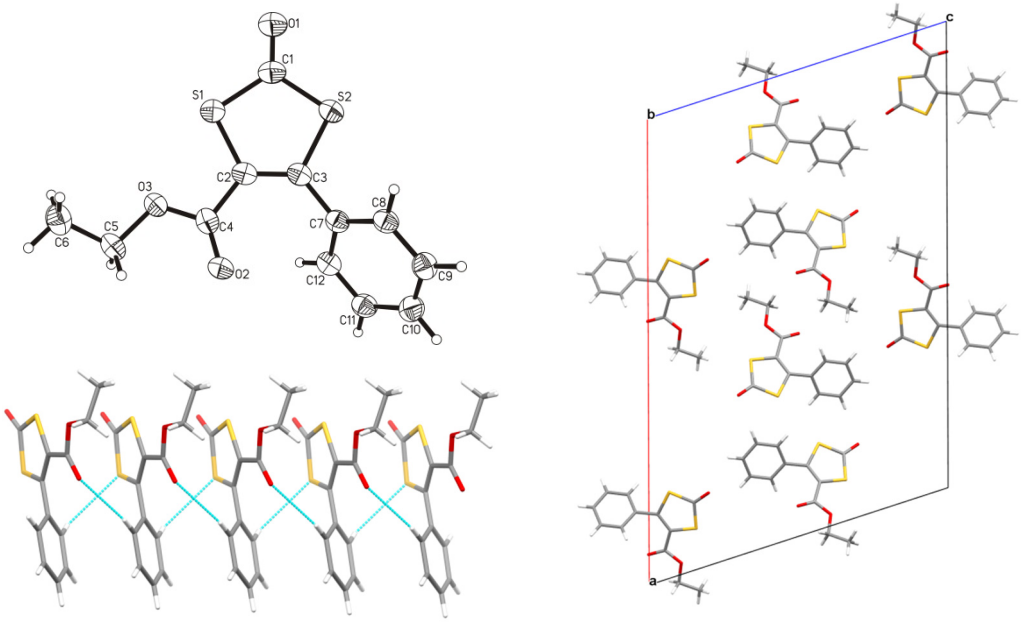

Figure 1. Top left: Molecular structure of **3** shown with 50% probability thermal ellipsoids. Selected bond lengths (Å) and angels (°): [C1–O1: 1.221(5), S1–C1: 1.761(4), S1–C2: 1.756(4), S2–C1: 1.764(4), S2–C3: 1.747(4), C2–C3, 1.353(5)]; [C2–C3–S2: 96.10(19), C3–C2–S1: 97.27(19), S1–C1–S2: 123.8(3)]. Bottom left: Non-classical intermolecular hydrogen bonding interactions (shown in light blue) forming chains, which protrude along the crystallographic *b*-axis (carbon: gray, hydrogen: white, oxygen: red, and sulfur: yellow). Right: Projection view of the crystal packing along the crystallographic *b*-axis.

The nickel cluster as part of **4** was first synthesized unintentionally, and then on purpose, by reacting nickel(II) chloride with the de-protected form of **3**, i.e., the $ecpdt^{2-}$ ligand, which was generated in situ by the addition of KOH in dry and degassed MeOH (Scheme 2). This reaction with the typical 2:1 stoichiometry, using molecular oxygen in air as the oxidant, usually leads to a nickel(III) bis-dithiolene complex, which had been the original target and was planned to be used in a dithiolene *trans*-metalation reaction. Here, however, an unexpected transformation took place. The raw product

was initially obtained upon drying as a brownish powder and then recrystallized by the slow diffusion of diethyl ether into an acetonitrile solution of **4** at room temperature while exposed to air, yielding black cube-shaped crystals with a reddish shine. The molecular structure of the Ni-tetrameric anion of **4** is shown in Figure 2, while all components of the crystal structure are displayed to the left in Figure 3.

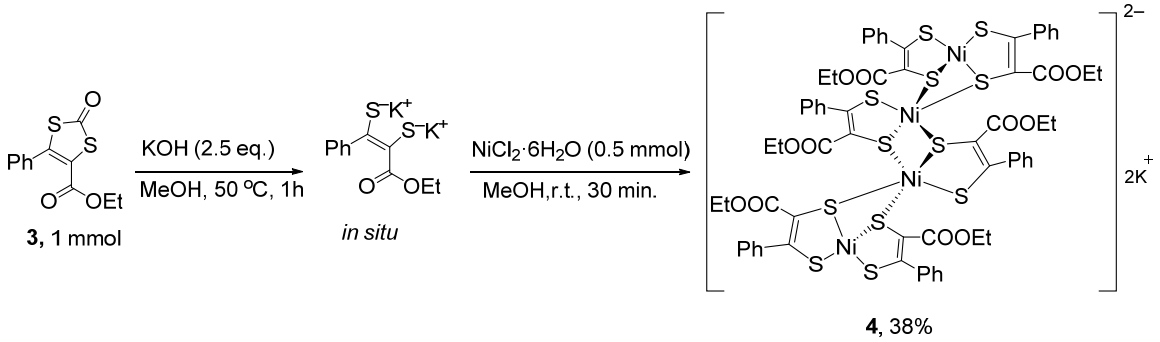

Scheme 2. Preparation of the nickel-tetramer salt $K_2[Ni_4(ecpdt)_6]$ (**4**) (Et = ethyl, Ph = phenyl).

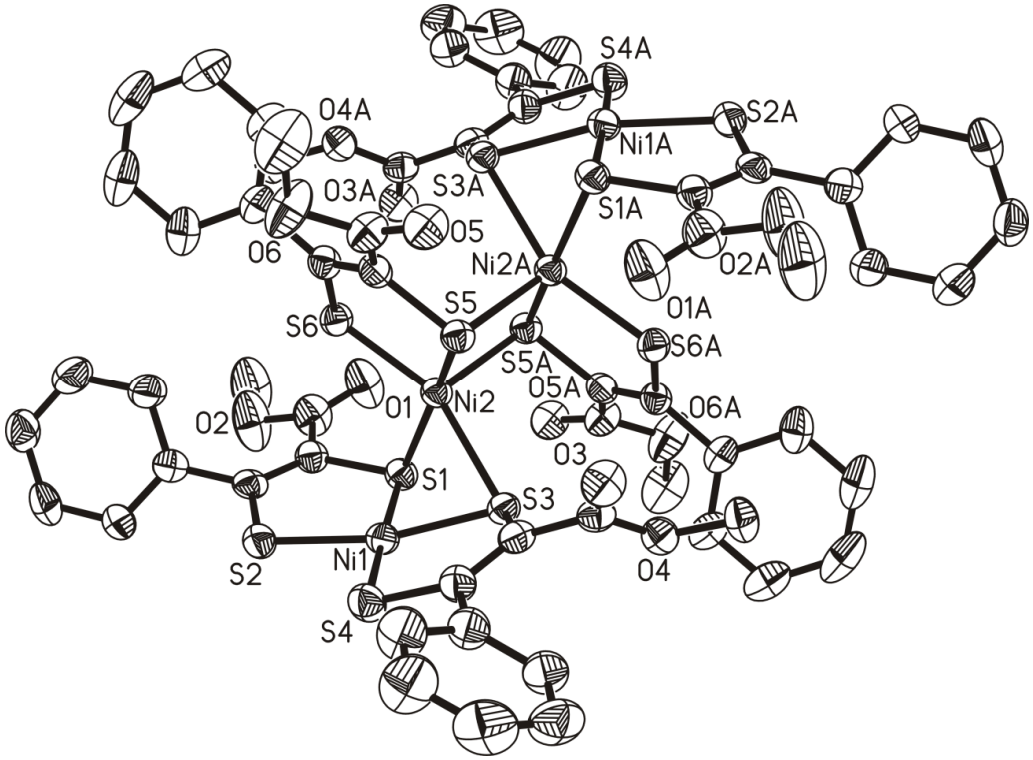

Figure 2. Molecular structure of the di-anion of **4·2CH$_3$CN·2Et$_2$O** shown with 50% probability thermal ellipsoids (the two potassium counter cations, disordered minor occupancies, H atoms, and lattice solvents are omitted and only heteroatom labels are shown for clarity reasons; see the Supplementary Material, Figure S16, for a fully labeled version; label extension A refers to symmetry (1−x, 1−y, 1−z) generated atoms).

4·2CH$_3$CN·2Et$_2$O crystallizes in monoclinic space group $P2_1/n$. The asymmetric unit consists of half the tetrameric di-anion, one potassium cation, one acetonitrile, and one diethyl ether. The complete molecular structure is generated by a symmetry operation (i.e., inversion in the center of the unit cell; 1−x, 1−y, 1−z). The unit cell of **4·2CH$_3$CN·2Et$_2$O** contains a total of two di-anions and four potassium ions as counter cations, although one anion is located in the very center. Each of the potassium ions is coordinated by one dithiolene ligand's sulfur donor atom plus three carbonyl oxygen donor atoms of the ester substituents (all belong to the Ni-tetrameric di-anion), as well as by one nitrogen donor

atom and another oxygen donor atom from the two coordinated solvent molecules (acetonitrile and diethyl ether), thereby resulting in a coordination number of six for the potassium cations (Figure 3). The four nickel centers of the anion are arranged in-line and the whole complex and entire structure are centrosymmetric. Selected bond lengths and angles of the anionic tetrameric nickel complex of **4** are listed in Table 1.

Table 1. Selected bond lengths [Å] and angles [°] for **4·2CH$_3$CN·2Et$_2$O** (label extension A refers to symmetry (1−x, 1−y, 1−z) generated atoms; all data are presented in the Supplementary Material, Table S2).

Bond Lengths		Bond Angles	
Ni(1)–Ni(2)	2.6747(11)	S(1)–Ni(1)–S(2)	91.82(6)
Ni(2)–Ni(2A)	2.9187(16)	S(1)–Ni(1)–S(3)	84.52(6)
Ni(1)–S(1)	2.1487(17)	S(1)–Ni(1)–S(4)	176.32(7)
Ni(1)–S(2)	2.1482(17)	S(1)–Ni(2)–S(3)	77.09(6)
Ni(1)–S(3)	2.1725(17)	S(1)–Ni(2)–S(5)	164.00(6)
Ni(1)–S(4)	2.1464(18)	S(1)–Ni(2)–S(5A)	95.06(6)
Ni(2)–S(1)	2.3125(16)	S(1)–Ni(2)–S(6)	92.80(6)
Ni(2)–S(3)	2.3509(16)	S(3)–Ni(2)–S(5)	94.06(6)
Ni(2)–S(5)	2.1758(16)	S(3)–Ni(2)–S(5A)	102.43(5)
Ni(2)–S(5A)	2.3554(16)	S(3)–Ni(2)–S(6)	156.26(6)
Ni(2)–S(6)	2.1793(16)	S(5)–Ni(2)–S(5A)	99.91(6)
C(1)–C(4)	1.366(8)	S(5)–Ni(2)–S(1)	90.24(6)
C(11)–C(14)	1.364(8)	Ni(1)–Ni(2)–S(5)	113.74(5)
C(21)–C(24)	1.369(8)	Ni(1)–Ni(2)–S(5A)	136.58(5)
		Ni(1)–Ni(2)–Ni(2A)	152.41(4)

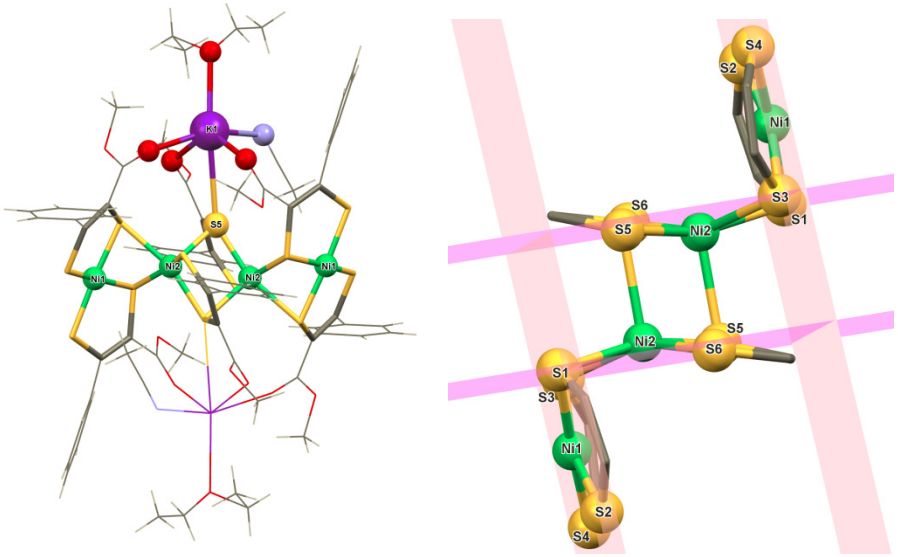

(**a**) (**b**)

Figure 3. (**a**) The entire molecular structure of crystalline $K_2[Ni_4(ecpdt)_6]\cdot 2CH_3CN\cdot 2Et_2O$ (**4·2CH$_3$CN·2Et$_2$O**) highlighting all contacts around the three distinct metal centers (Ni1, Ni2, and K1); disordered minor occupancies not shown; carbon: gray, hydrogen: white, oxygen: red, sulfur: yellow, nickel: green, and potassium: purple. Selected bond lengths in Å: K1–O1: 2.591(5), K1–O3: 2.651(5), K1–O5: 2.676(5), K1–O7: 2.744(8), K1–S5: 3.378(2), and K1–N1: 2.831(8); (**b**) arrangement of nickel centers and coordinated dithiolene ligands (the ligand substituents are omitted for clarity); notably, the Ni2 centers are slightly dislocated above and below the S1, S3, S5, and S6 planes (darker pink), while Ni1 resides more firmly in the plane (brighter pink) of its four surrounding sulfur donor atoms (S1, S2, S3, and S4).

The average Ni–S distance for Ni1 (the outer square-planar nickel center) is 2.154 Å, while the three distances range from 2.1464 Å to 2.1487 Å and one is notably longer, with a value of 2.1725 Å

(S3). For Ni2 (the inner square-pyramidal nickel center), the average bond length is 2.275 Å and the distances can be divided into two sets. One dithiolene ligand is only coordinated to Ni2 and has no interaction with Ni1. The respective Ni–S distances are 2.1758 Å (S5) and 2.1793 Å (S6). S5 binds to both Ni2; once in a basal position as part of the ene-dithiolate chelate and secondly in a bridging fashion (Ni2–S5–Ni2) occupying the apex of the second nickel's pyramidal coordination polyhedron. The distance to this second Ni2 is 2.3554 Å. The other two Ni2–S distances each involve one sulfur donor atom of the two dithiolene ligands forming chelates with Ni1 (Ni2–S1: 2.3125 Å and Ni2–S3: 2.3509 Å). Conspicuously, both S1 and S3 belong to the ester sides of the dithiolene ligands (not the phenyl side). All individual and average Ni–S distances are longer for the inner five-coordinated nickel centers than they are for the outer four-coordinated nickel centers. This points to Ni1 being smaller, with a more oxidized center, and Ni2 being larger and more reduced. This contrasts with the nearly perfectly square-planar geometry around Ni1 being most often associated with a d^8 metal center (i.e., corresponding to more reduced Ni^{2+}). At the same time, the coordination shell around Ni2 is more crowded, engaging five instead of only four ligands. This might contribute to elongation of the Ni–S bonds, despite a higher oxidation state. Notably, the longer ones of the Ni–S bonds, i.e., those which surpass 2.3 Å, mean that the Ni and S atoms have distances which are longer than the sum of their covalent radii (2.29 Å [53]), suggesting only comparably weak attraction/interaction. While Ni1 is clearly strongly coordinated by all four sulfur donor atoms of its two dithiolene ligands, three out of the five Ni–S interactions of Ni2 are significantly weakened beyond a typical Ni–S single bond. The longest, and thus weakest, Ni–S distance is the one which holds the two identical halves of the tetramer together, i.e., the apical coordination of S5 to the second Ni2 in the complex's center. Notably, S5 not only bridges the two Ni2 centers, but also interacts with the potassium counter ion (S5–K1: 3.378(2) Å). This distance is very close to the sum of their covalent radii (3.39 Å [53]) and it will take away at least some electron density from the Ni2–S5 bonds, thereby weakening them. The longer nickel–sulfur bonds are, in fact, consistent with a dissociation (vide infra) of the tetrameric complex in solution, as has been observed previously for dimeric species with different central metals, which are closely related to the central structural Ni2/Ni2 motif of **4·2CH$_3$CN·2Et$_2$O** [54,55]. The central Ni2–Ni2A distance across the perfectly planar, lozenge-shaped four-membered ring (formed with two S5 sulfur bridges) is with 2.9178(15) Å longer than the Ni1–Ni2 distance of 2.6750(10) Å. The observed Ni–Ni distances are both in the range, yet slightly shorter compared to the respective distances in the previously described related $[Ni_4(\alpha\text{-tpdt})_6]^{2-}$ complex (3.142(3) Å and 2.756(2) Å) [35]. Based on a detailed DFT computational study and due to the absence of bond critical points and the occupation of antibonding molecular orbitals, Neves et al. dismissed the presence of relevant Ni–Ni bonding in their Ni_4 species [35] and due to the very close similarity of the two tetrameric complexes, it can be assumed that there are no actual metal–metal bonds in **4·2CH$_3$CN·2Et$_2$O** either.

With regard to assigning the two oxidation states (+2 and +3) to the inner and outer nickel centers, metrical structural parameters of the C–S and C=C bonds in the three dithiolene ligands of the asymmetric unit are also of interest. Dithiolene ligands are non-innocent and can push more electron density than usual towards a coordinated metal ion using their π system, including the lone pairs in the sulfur *p*-orbitals (see the review by Yang et al. in Special Issue "Transition Metals in Catalysis: The Functional Relationship of Fe–S Clusters and Molybdenum or Tungsten Cofactor-Containing Enzyme Systems" of *Inorganics*) [54,56]. The ligand's extra electron density donation beyond a single coordinative σ-bond comes at the expense of the C=C double bond strength and is concurrent with the formation of a partial C=S bond character. Non-innocent behavior, therefore, results in slightly elongated C–C and slightly shortened C–S distances (with the latter quite often only being on one side of the ene-dithiolate ligand). Typically, the resultant bond lengths suggest a mixed single/double bond character for both interactions; most often residing more on the side of the ene-dithiolate forms.

In the protected ligand precursor **3**, the C=C double bond is 1.353(5) Å long and the C–S distances are 1.747(4) Å (phenyl side) and 1.756(4) Å (ester side) (see Table 2). In the ligand, which is only coordinated to Ni2 in **4·2CH$_3$CN·2Et$_2$O**, the double bond is elongated (C21–C24: 1.369(8) Å), the ester

side C–S distance is slightly shortened (C21–S5: 1.748(6) Å), and the phenyl side C–S distance is significantly shortened (C24–S6: 1.712(6) Å). This supports the presence of a moderate non-innocent effect and a sulfur-mediated push of electron density out of the C=C double bond towards the coordinated nickel center.

Table 2. Atom to atom distances [Å] of C=C and C−S bonds in ligand precursor **3** and complex salt **4·2CH$_3$CN·2Et$_2$O**.

3		**4·2CH$_3$CN·2Et$_2$O**	
C(2)–C(3)	1.353(5)	C(1)–C(4)	1.366(8)
C(2)–S(1) (ester side)	1.756(4)	C(1)–S(1) (ester side)	1.745(6)
C(3)–S(2) (phenyl side)	1.747(4)	C(4)–S(2) (phenyl side)	1.711(6)
		C(11)–C(14)	1.364(8)
		C(11)–S(3) (ester side)	1.749(6)
		C(14)–S(4) (phenyl side)	1.729(6)
		C(21)–C(24)	1.369(8)
		C(21)–S(5) (ester side)	1.748(6)
		C(24)–S(6) (phenyl side)	1.712(6)

Ni1 is firmly bound by two chelating dithiolene ligands. The respective ligands' bond lengths here also exhibit an elongation of the C=C distances (C1–C4: 1.366(8) Å, C11–C14: 1.364(8) Å), while the C–S distances are significantly shortened on the phenyl sides (C4–S2: 1.711(6) Å and C14–S4: 1.729(6) Å) and more subtly on the ester sides (C1–S1: 1.745(6) Å and C11–S3: 1.749(6) Å). Overall a non-innocent effect is present here as well, but to a lesser extent overall. Interestingly, for all three dithiolene ligands, the phenyl sides exhibit the shorter C–S distances, suggesting that this is the sulfur atom which moves more electron density towards the nickel center, even though it is, in all cases, the ester side of the dithiolene ligand which engages in bridging binding modes. This un-symmetrical trend has already been observed in the ligand precursor, but to a much lesser extent. Possibly, some type of push-pull effect is present here in the unsymmetrically substituted dithiolenes, which is strengthened upon coordination due to the ligands' non-innocent behavior. In a nickel ion with a higher oxidation state, the non-innocent effect is presumed to be more prominent compared to more reduced, i.e., electron-rich, metal centers. In contrast to the recorded Ni–S bond lengths, which suggest that the outer nickel ions (Ni1) are smaller (hence, more oxidized), the structural data of the dithiolene ligands, therefore, support Ni2 being more oxidized with a stronger push of electron density from ligands to metal. This paradox can only be solved by involving additional analytical methods and observations; in particular, the magnetic properties are helpful in this respect (vide infra).

The unexpectedly formed tetrameric nickel complex **4** was further analyzed by a set of standard/routine characterization methods. The most prominent molecular ion peaks in its ESI-MS spectrum, which was recorded in methanolic solution and in the negative ion mode, can be assigned to monomeric bis-dithiolene nickel(III) species with charge ratios (m/e) of 533.9, 519.9, and 505.8. The oxidation of the nickel(II) centers to nickel(III) is not uncommon/unexpected, given that the solution of the probe needs to be handled in air prior to being injected into the instrument. The observed isotopic patterns thus belong to complex fragmentations and oxidation of the outer nickel centers (for the two lower mass signals) and to transformations of one or two of the ethyl esters to methyl ester functional groups in the methanol solvent (see the Supplementary Material, Figure S9). This strongly supports the notion that some of the nickel sulfur bonds in the complex are decidedly weak and most likely rather easily severed when dissolved in a coordinating solvent. From this behavior, we can therefore derive qualitative approximations of Ni–S bond strengths (in particular for bridging binding modes) from metrical parameters, i.e., it can be concluded whether they have to be presumed short enough to be stable, despite the presence of potentially competing coordinating ligands or whether they are too long and thus labile.

Reported Ni–S distances in FeNi and FeNiSe hydrogenases range from rather short (1.98 Å) to quite long (2.6 Å) [57–62]. It has to be taken into consideration, though, that the accuracy of such metrical parameters, particularly in proteins, greatly depends on the resolution of the gathered data. Naturally, the most recent published values tend to be the most accurate ones and they rest on the shorter side. In reports where the Ni–S distances are distinguished, apical and bridging ones are typically longer (up to 2.6 Å in comparison to shorter terminal ones of 2.2–2.3 Å), as expected. Bond lengths of 2.4 Å are long enough to suggest that they are labile and easily severed. The respective structural studies, however, are less recent. When compared to the observations of this study, the most recent published Ni–S bond lengths from an FeNiSe hydrogenase (1.98 Å, PDB code: 5JSH) strongly suggest that the respective interactions between the nickel center and sulfur donor atom are stable and have no tendency to dissociate [61]. Notably, in a recent comprehensive theoretical investigation [63] based on the most recent X-ray structure of an FeNiSe hydrogenase, the theoretical values were ca. 0.2 Å longer than the experimental ones and from a chemical point of view, the computed bond lengths were actually more reasonable for a Ni^{2+} or Ni^{3+} centre. However, these slightly longer computational bonds are decidedly shorter than the bonds in the Ni tetrameric structure of this study, which can apparently lead to a break-down of the complex in solution. This renders any potential mechanism in nickel-bearing hydrogenases less likely, which would involve replacing a Ni–S contact with an incoming donor atom.

Infrared spectra of **4** were recorded both in the solid-state (KBr matrix) and in solution (CH_3CN) (see the Supplementary Material, Figure S10). Assignment of the observed vibrational bands is based on a comparison with the ligand precursor's IR spectrum and on an extensive previous respective report [64]. Vibrational bands are indeed shifted, significantly in parts, in the solid-state spectrum compared to the solution spectrum. In particular, the Ni–S band (~550 cm^{-1}) and the C–S band (~1000 cm^{-1}) regions show fewer and less intense signals in solution than in the solid-state. This indicates considerable changes in the molecular and/or electronic structures upon dissolving, which is again in accordance with the proposed dissociation of the tetrameric species into dimers or monomers in solution.

The electronic absorption spectra of **4** were recorded in MeOH, CH_3CN, and water solvent (see the Supplementary Material, Figure S11). The broad low-energy near-IR band at 868 nm is very characteristic of monomeric bis-dithiolene nickel complexes with oxidation states of +3 or +4 and has been ascribed to transitions of sulfur lone pair electrons into mixed nickel-ligand molecular orbitals which are empty (OS +4) or singly occupied (OS +3), while Ni^{2+} bis-dithiolene complexes do not exhibit this transition because the respective receiving MO is already fully occupied [29,65–67]. Notably, this transition is missing in the aqueous spectrum, which means that either the tetrameric complex does not dissociate in water; it dissociates completely, even beyond the bis-dithiolene species to, for instance, mono-dithiolene species; or it is being reduced/not oxidized in aqueous solution. There is no reasonable explanation for why water as a medium would be better at protecting the tetrameric complex's fragments against oxidation by air or even induce reduction compared to acetonitrile or methanol. The most likely explanation is that water not only disintegrates the tetrameric complex into monomers by replacing the weaker bound sulfur donor atoms around the inner Ni2, but also interferes with the coordination shell of the outer Ni1, so that no bis-dithiolene complexes result from dissolving in water. The spectra in methanol and acetonitrile are slightly distinct, which suggests that interactions between solvent and dissolved species take place and result in subtle differences in the electronic structures of the mono-dithiolene fragments, which mix in the resulting solutions with the bis-dithiolene complexes.

The electrochemical properties of **4** were investigated by cyclic voltammetry (CV; referenced versus ferrocene, Fc/Fc^+, in CH_3CN solution with 0.1 M of $[^nBu_4N][PF_6]$ as supporting electrolyte; see the Supplementary Material, Figures S12 and S13). The voltammograms are relatively close to those of *bis*-dithiolene nickel complexes available in the literature [29,30], again supporting a dissociation of the tetrameric complex into monomers (or dimers). The two observed quasi-reversible redox transitions are, hence, tentatively ascribed to the couples $[Ni(ecpdt)_2]^{2-}/[Ni(ecpdt)_2]^-$ and $[Ni(ecpdt)_2]^-/[Ni(ecpdt)_2]^0$

at −1.1 and −0.1 V (vs. Fc/Fc^+), respectively. However, the evaluation here is impeded, due to the possible chemical dissociation equilibria and potentially manifold species, which may occur in solution. Neves et al. have also investigated their related tetrameric nickel complex electrochemically and reported two redox transitions at −0.480 V and +0.286 V vs. Ag/AgCl [35], which roughly translates into values of −0.68 V and +0.08 V vs. Fc/Fc^+ [68]. These values are, firstly, more positive and their complex is thus easier to reduce. Secondly, the gap between the two redox events is smaller by ca. 0.24 V, suggesting a more significant involvement of the dithiolene ligand in the redox transitions than in the case of **4**. While we do not observe any further distinguishable signals, Neves et al. further reported a redox process in between at −0.095 V vs. Ag/AgCl (−0.298 vs. Fc/Fc^+) [35]. Overall, however, the electrochemical behavior of the two tetrameric complexes is very similar, particularly when considering that different solvents were used.

Lastly, in order to also unambiguously assign the oxidation states +2 and +3 to the appropriate nickel centers in **4**, an investigation of the magnetic properties of the complex was carried out with comparably simple/convenient methods. This was done in both the solid-state and in solution. For the solid-state investigation, a Magnetic Susceptibility Balance (MSB), also referred to as a Guy Balance, was used. Based on the measurement data, the magnetic moment was determined as μ_{eff} = 1.86 *BM* (Bohr magneton; see the Supplementary Material for calculation details) per non-dissociated tetrameric nickel complex. Therefore, **4** exhibits some paramagnetism, but much less than anticipated for the two unpaired electrons of the two Ni(III) centers, and only slightly more than the expected spin-only magnetism for a single unpaired electron of 1.73 BM. This clearly points toward significant antiferromagnetic coupling in the solid-state between the two metal centers and this can only take place if the respective atoms are close together. These observations, therefore, very clearly place the unpaired electrons on the two central nickel ions (Ni2), which are thus assigned the oxidation state +III. This is in accordance with the metrical structural ligand data and fits the results of the DFT study by Neves et al. on the related tetrameric complex perfectly well, including the predicted antiferromagnetic coupling [35]. Notably, Neves et al. did not have enough material to conduct a respective experiment with their complex. With our experimental data, we can confirm their computational results and vice versa, even though the complexes are not strictly identical.

The magnetic moment of **4** in solution was determined by the Evans method [69,70]. μ_{eff} of **4** was calculated to be 2.826 BM (see the Supplementary Material for details of measurements and calculations). The effective magnetism is, hence, in solution almost perfectly equal to the spin-only value for two unpaired electrons (2.828 BM) per tetrameric complex. This points towards two d^7/Ni(III) centers with one unpaired electron each, which are not antiferromagnetically coupled in solution, as opposed to what is observed in the solid-state. Again, the distinct magnetic properties in solution and in the solid-state firmly support the fragility of the central (long) Ni–S bonds and a dissociation of the tetramer upon interaction with a solvent.

3. Materials and Methods

3.1. Physical Measurements

NMR measurements were recorded on a Bruker Avance II-300 MHz instrument (Karlsruhe, Germany). All samples were dissolved in deuterated solvents, and chemical shifts (δ) are given in parts per million (ppm) using solvent signals as the reference ($CDCl_3$ 1H: δ = 7.24 ppm; 13 C: δ = 77.0 ppm) related to external tetramethylsilane (δ = 0 ppm). Coupling constants (*J*) are reported in Hertz (Hz), and splitting patterns are designated as s (singlet), d (doublet), t (triplet), q (quartet), quint (quintet), m (multiplet), and dd (doublet of doublet). The infrared spectra were recorded on a Perkin-Elmer Fourier-Transform Infrared (FT-IR) spectrophotometer in the range of 4000–400 cm^{-1} using KBr pellets (solid-state) or KBr windows and a concentrated CH_3CN solution of the analyte (in solution). Assignment of the bands was done with subjective appreciation: w = weak, m = medium, s = strong, vs = very strong, and br = broad. UV/vis spectra were recorded on a Shimadzu UV-3600PC

spectrophotometer. Solutions with concentrations ranging from 10 to 1 μM were prepared for the measurements. All measurements were carried out at room temperature in quartz cuvettes (path length = 1 cm). Elemental analyses (C, H, N, and S) were carried out with an Elementar Vario Micro Elemental Analyzer (Langenselbold, Germany). Mass spectra (APCI and ESI) were recorded with an Advion Expression CMS spectrometer (Ithaca, NY, USA) with a resolution of 0.5–0.7 m/e units (FWHM) at 1000 m/e units s^{-1} over the entire acquisition range. The magnetic moment experiment was performed with a Johnson-Matthey Mark I Magnetic Susceptibility Balance (Redwitz, Germany). Electrochemical measurements were carried out with an AUTOLAB PGSTAT12 potentiostat/galvanostat (Filderstadt, Germany) using a glassy carbon disc electrode with a reaction surface of 1 mm^2 as the working electrode. A platinum knob electrode (together with internal referencing versus ferrocene/ferrocenium (Fc/Fc+)) was used as a reference electrode and a platinum rod electrode was employed as an auxiliary electrode. All measurements were carried out inside a glove box and controlled with the NOVA software (2.0.1., Metrohm, Filderstadt, Germany). Tetrabutylammonium hexafluorophosphate (0.1 M; electrochemical grade from Fluka, München, Germany) was used as the electrolyte.

3.2. X-Ray Crystallography

Suitable single crystals of **3** and **4·2CH$_3$CN·2Et$_2$O** were mounted on a thin glass fiber coated with paraffin oil. X-ray single-crystal structural data were collected using a STOE-IPDS II diffractometer (Darmstadt, Germany) equipped with a normal-focus, 2.4 kW, sealed-tube X-ray source with graphite-monochromated Mo Kα radiation (λ = 0.71073 Å) at low temperature (170 K). The program XArea was used for the integration of diffraction profiles; numerical absorption corrections were carried out with the programs X-Shape and X-Red32, all from STOE© ((Darmstadt, Germany). The structures were solved by direct methods with SHELXT [71] and refined by full-matrix least-squares methods using SHELXL [72]. All calculations were carried out using the WinGX system, Ver 2018.3 [73]. All non-hydrogen atoms were refined anisotropically. The hydrogen atoms were refined isotropically on calculated positions using a riding model with their Uiso values constrained to 1.2 Ueq of their pivot atoms for methyl groups and 1.2 Ueq of their pivot atoms for all other groups. The refinement of the crystallographic data of **3** was unremarkable. In the refinement of **4·2CH$_3$CN·2Et$_2$O**, several disorder problems were encountered. The two solvent molecules coordinated to K1 exhibited thermal motion and the respective ellipsoids were comparably large. For acetonitrile, the three non-hydrogen atoms were constrained with SIMU and DELU. In addition, the ethyl groups of Et_2O were disordered over two positions each, which was treated with SADI, SIMU, and DELU constraints. Furthermore, two out of three ethyl groups of the dithiolene ethyl ester functionalities were disordered over two positions each. Again, this was treated with SADI, SIMU, and DELU constraints.

General crystallographic, crystal, and refinement data for **3** and **4·2CH$_3$CN·2Et$_2$O** are provided in the supplementary data file (see the Supplementary Material, Table S1). Crystallographic data were deposited with the Cambridge Crystallographic Data Centre, CCDC, 12 Union Road, Cambridge CB21EZ, UK. These data can be obtained free of charge upon quoting the depository numbers CCDC 1985587 (**3**) and 1985588 (**4·2CH$_3$CN·2Et$_2$O**) by FAX (+44-1223-336-033), email (deposit@ccdc.cam.ac.uk), or their web interface (at http://www.ccdc.cam.ac.uk).

3.3. Syntheses

3.3.1. Ethyl 2-bromo-3-oxo-3-phenylpropanoate (**1**)

Method (a). Ethyl benzoylacetate (10 g, 52 mmol) and *N*-bromosuccinimide (NBS) (9.26 g, 52 mmol) were triturated together in a porcelain mortar for 15 min. The resulting liquid paste was allowed to stand for 3 h and then washed three times with 100 mL H_2O in a separating funnel. The final crude product was distilled by Kugelrohr distillation to remove the unreacted starting material. Distillation was performed at 70 °C under a vacuum of 100 mmHg (b.p. 135 °C). The final product was a pale yellow oil that is a severe lachrymator. Yield: 6.34 g, 45%.

Method (b). NBS (9.26 g, 52 mmol) was added to ethyl benzoyl acetate (10 g, 52 mmol). The reaction mixture was refluxed one hour under microwave heating (magnetron power of 750 W until a temperature of 160 °C was reached). The dark brown reaction mixture was cooled slowly for 30 min and was distilled by Kugelrohr distillation. Yield: 10 g, 71%. ^{1}H NMR ($CDCl_3$, 300 MHz): δ, ppm = 7.94–8.05 (m, ortho-phenyl, 2H), 7.55–7.67 (m, para-phenyl, 1H), 7.43–7.54 (m, meta-phenyl, 2H), 5.73 (s, –CHBr, 1H), 4.27 (q, *J* = 6.9 Hz, $–CH_2$, 2H), 1.23 ppm (t, *J* = 7.2 Hz, $–CH_3$, 3H). ^{13}C NMR ($CDCl_3$, 75 MHz): δ, ppm = 187.9 (PhC=O), 164.8 (C=O), 134.0 (C-phenyl), 133.0 (C-phenyl), 128.8 (C-phenyl), 128.6 (C-phenyl), 62.9 (CH_2), 46.2 (CHBr), 13.5 (CH_3). APCI-MS (EI+): m/e calculated for $C_{11}H_{11}BrO_3$: 269.99, Found: 270.99 ($[M + H]^+$).

3.3.2. Ethyl 2-(isopropoxycarbonothioylthio)-3-oxo-3-phenylpropanoate (**2**)

Potassium o-isopropyl xanthate (3.34 g, 19.1 mmol) was added portion-wise to a solution of **1** (4.33 g, 16 mmol) dissolved in 60 mL acetone. The red mixture was heated at 50 °C for 1 h and then stirred overnight at RT. Precipitated white KBr was filtered off with suction employing Celite. The brown-yellow solution was concentrated on a rotary evaporator, and the red oil was dissolved in chloroform. The organic phase was washed with 10% HCl and water, and dried over anhydrous Na_2SO_4, and the solvent was evaporated on a rotary evaporator, resulting in a reddish-brown oil that was used without further purification. Yield: 4.4 g, 84%. APCI-MS (EI+): m/e calculated for $C_{12}H_{12}O_4S_2$: 284.02, Found: 284.65 ($[M + H]^+$).

3.3.3. 4-Ethylcarboxylate-5-phenyl-1,3-dithiole-2-one (**3**)

A total of 20 mL of sulfuric acid was slowly added to an ice-cold solution of **2** (4.09 g, 12.5 mmol) in 75 mL of Et_2O:DCM solvent mixture (1:1 ratio) and was stirred overnight at RT. The reaction was controlled by TLC (*n*-hexane/EtOAc). The solution was cooled down in an ice bath and slowly poured onto ice-cooled H_2O (200 mL). The solution was stirred for another hour and then extracted with CH_2Cl_2 (3 × 50 mL), dried over anhydrous Na_2SO_4, and concentrated on a rotary evaporator to produce a crude, dark red oil that was purified by flash column chromatography with gradient elution (5–15% EtOAc) to afford **3** as colorless crystals. Yield: 2.2 g, 63% (considering remaining 1/16 molecule of *n*-hexane and EtOAc per formula each, as supported by NMR and EA). ^{1}H NMR ($CDCl_3$, 300 MHz): δ, ppm = 7.31–7.54 (m, phenyl, 5H), 4.13 (q, *J* = 7.2 Hz, $–CH_2$, 2H), 1.12 ppm (t, *J* = 7.0 Hz, $–CH_3$, 3H). ^{13}C NMR ($CDCl_3$, 75 MHz): δ, ppm = 188.3 ($C{=}O_{dithiolene}$), 159.0 ($C{=}O_{ester}$), 145.5 (Ph–$C{=}C_{dithiolene}$), 131.0 (C-phenyl), 129.8 (C-phenyl), 128.9 (C-phenyl), 128.3 (C-phenyl), 119.9 (COOEt–$C{=}C_{dithiolene}$), 62.1 (CH_2), 13.7 (CH_3). FT-IR (KBr): (ν, cm^{-1}) = 3421 (br), 3005 (ws), 2980 (s), 1728 (s), 1695 (s), 1674–1658 (br), 1543 (s), 1489 (m), 1471(s), 1444 (m), 1390 (s), 1363 (w), 1263–1253 (br), 1205 (m), 1155 (m), 1109 (s), 1087 (w), 1066 (w), 1033 (m), 1020 (s), 948 (m), 912 (m), 893 (s), 867 (m), 825 (w), 802 (w), 761 (w), 748 (m), 727 (w), 690 (w), 628 (w), 588 (w), 591 (w), 491 (w), 466 (w), 445 (w). Elemental analysis for $C_{12}H_{10}O_3S_2{\cdot}1/16C_4H_8O{\cdot}1/16C_6H_{14}$ ($C_{12.625}H_{11.375}O_{3.063}S_2$; M = 277.23 g/mol) calc.: C, 54.70; H, 4.14; S, 23.13. Found: C, 55.30; H, 4.04; S, 22.73. APCI-MS (EI+): m/e calculated for $C_{12}H_{10}O_3S_2$: 266.01, Found: 266.94 ($[M + H]^+$). Fragmentation calc. for $C_{10}H_6O_3S_2$: 237.98, Found: 238.97 ($[M + H]^+$).

3.3.4. $K_2[Ni_4(ecpdt)_6]\cdot 2CH_3CN{\cdot}2Et_2O$ (**$4{\cdot}2CH_3CN{\cdot}2Et_2O$**)

A total of 0.15 g of **3** (0.56 mmol) was suspended with 78 mg of KOH (1.4 mmol, 2.5 equiv.) in 10 mL of degassed methanol and stirred under nitrogen for 1 h at 50 °C, affording an orange solution. Next, 3 mL of a solution of $NiCl_2{\cdot}6H_2O$ (0.5 mmol, 0.12 g) in methanol was added, and the resulting reaction mixture was stirred for 30 min. Then, it was concentrated to dryness, affording a dark brown colored precipitate. Single crystals were obtained by recrystallization from a solvent mixture of CH_3CN:Et_2O (ratio 1:2) in a diethyl ether saturated atmosphere, while air was allowed to slowly diffuse in, providing molecular oxygen needed for the partial oxidation of nickel centers. Yield: 90 mg, 38%. FT-IR (KBr): ν, cm^{-1} = 3446 (br), 3055 (w), 2974 (s), 1668 (br), 1365–1473 (s), 1132–1303 (br), 985–1062 (m), 804 (w), 744 (w), 696 (w), 657 (w), 617 (m), 503 (m). ESI-MS (EI−): m/e calculated for $C_{20}H_{16}NiO_4S_4$ $[M]^-$ (*i*): 505.9, found: 505.0; calc. for $C_{21}H_{18}NiO_4S_4$ (*ii*): 519.9, found: 519.0, calc. for $C_{22}H_{20}NiO_4S_4$ (*iii*): 533.9,

found: 533.0. *N.B.*: there appear to be signals in the mass spectrum supporting fragments much larger than monomers, but they are of a very low intensity. UV-Vis (CH_3CN): λ_{max} (ε/M^{-1} cm^{-1}), nm = 256, 315, 366, 476, 518, 868 (2000). Cyclic voltammetry (in CH_3CN, Bu_4NPF_6 vs. Fc/Fc+): $E_{1/2}$ = −1.1 V ($E^2_{p,c}$), −0.1 V ($E^1_{p,c}$).

Note: parts of the study/experiments were included in the recent Ph.D. thesis of Mohsen Ahmadi [74].

4. Conclusions

In conclusion, an unexpected di-anionic, tetra-nuclear in-line, hetero-valent, centrosymmetric nickel dithiolene complex was synthesized, which had only one precedent in the literature. The employed dithiolene ligand was substituted unsymmetrically (Ph, –COOEt), probably inducing/experiencing a mild push-pull effect, which was intensified upon coordination. The compound's crystal structural data was evaluated in detail. Comparing the large range of observed Ni–S bond distances will facilitate the evaluation of respective bond strengths in nickel- and sulfur-dependent enzymes' active sites. The two distinct oxidation states +2 and +3 could be assigned unambiguously to the outer and inner nickel centers, respectively, by determining the complex's effective magnetism (μ_{eff}) and by consulting previously published computational results of a related compound. It was further established by several spectroscopic and other methods that the tetramer due to the comparably labile Ni–S bonds in its center dissociates in solution, either into identical dimers or, more likely, into two sets of distinct monomers. Previous computational results without an experimental backup regarding the assignment of oxidation states and antiferromagnetic coupling in the tetramer's solid-state could be verified experimentally (and vice versa) with this novel complex.

Supplementary Materials: The following are available online at http://www.mdpi.com/2304-6740/8/4/27/s1: Figure S1: ^{1}H NMR of **1**; Figure S2: ^{13}C NMR of **1**; Figure S3: APCI mass spectrum of **1**; Figure S4: APCI mass spectrum of **2**; Figure S5: ^{1}H NMR of **3** (*ecpdt*); Figure S6: ^{13}C NMR of **3**; Figure S7: APCI mass spectrum of **3**; Figure S8: FT-IR spectrum of **3**; Figure S9: The ESI(−)-MS of **4**; Figure S10: IR spectra of **4**; Figure S11: UV-vis-NIR spectra of **4** and extinction coefficient diagram; Figure S12: Cyclic voltammogram of **4**; Figure S13: Cyclic voltammogram of **4** at different scan rates; Figure S14: ^{1}H NMR for magnetic moment measurement of the Ni cluster; Figure S15: ^{1}H NMR for magnetic moment measurement of the standard; Table S1: General crystallographic data of **3** and **4·2CH$_3$CN·2Et$_2$O**; Figure S16: Molecular structure of the di-anion of **4·CH$_3$CN·Et$_2$O** shown with 50% probability thermal ellipsoids (the two potassium counter cations, disordered minor occupancies, H atoms, and lattice solvents are omitted for clarity); Table S2: Complete list of bond lengths [Å] and angles [°] for **4·2CH$_3$CN·2Et$_2$O**; Table S3: Hydrogen-bond geometry [Å and °] of **4·2CH$_3$CN·2Et$_2$O**; Table S4: Atomic coordinates and equivalent isotropic displacement parameters for **4·2CH$_3$CN·2Et$_2$O**; Table S5: Anisotropic displacement parameters (Å^2 × 10^3) for **4·2CH$_3$CN·2Et$_2$O**; Cif and checkcif files of **3** and **4·2CH$_3$CN·2Et$_2$O**.

Author Contributions: Synthesis, characterization, and manuscript draft, M.A.; additional investigation, validation, and manuscript draft, J.C.; crystallography, N.C. and C.S.; conceptualization, writing—review and editing, and resources, C.S.; all authors have read and agreed to the published version of the manuscript. All authors have read and agreed to the published version of the manuscript.

Funding: This research was funded by the DFG (Deutsche Forschungsgemeinschaft), grant number SCHU 1480/4-1, as part of the SPP 1927 (Priority Program) "Iron-Sulfur for life". The financial support is gratefully acknowledged.

Acknowledgments: The authors thank Marlen Redies and Gabriele Thede for carrying out the EA and NMR measurements.

Conflicts of Interest: The authors declare no conflicts of interest.

References

1. Schrauzer, G.N.; Mayweg, V.P. Preparation, Reactions, and Structure of Bisdithio-α-diketone Complexes of Nickel, Palladium, and Platinum. *J. Am. Chem. Soc.* **1965**, *87*, 1483. [CrossRef]
2. Schrauzer, G.N.; Mayweg, V. Reaction of Diphenylacetylene with Nickel Sulfides. *J. Am. Chem. Soc.* **1962**, *84*, 3221. [CrossRef]
3. Eisenberg, R.; Stiefel, E.I.; Rosenberg, R.C.; Gray, H.B. Six-Coordinate Trigonal-Prismatic Complexes of First-Row Transition Metals1. *J. Am. Chem. Soc.* **1966**, *88*, 2874–2876. [CrossRef]

4. Stiefel, E.I.; Eisenberg, R.; Rosenberg, R.C.; Gray, H.B. Characterization and Electronic Structures of Six-Coordinate Trigonal-Prismatic Complexes. *J. Am. Chem. Soc.* **1966**, *88*, 2956–2966. [CrossRef]
5. Balch, A.L.; Dance, I.G.; Holm, R.H. Characterization of dimeric dithiolene complexes. *J. Am. Chem. Soc.* **1968**, *90*, 1139–1145. [CrossRef]
6. Mueller-Westerhoff, U.T.; Vance, B.; Yoon, D.I. The synthesis of dithiolene dyes with strong near-IR absorption. *Tetrahedron* **1991**, *47*, 909–932. [CrossRef]
7. Winter, C.S.; Oliver, S.N.; Manning, R.J.; Rush, J.D.; Hill, C.A.S.; Underhill, A.E. Non-linear optical studies of nickel dithiolene complexes. *J. Mater. Chem.* **1992**, *2*, 443–447. [CrossRef]
8. Oku, H.; Ueyama, N.; Kondo, M.; Nakamura, A. Oxygen atom transfer systems in which the (*m*-oxo)dimolybdenum(V) complex formation does not occur: Syntheses, structures, and reactivities of monooxomolybdenum(IV) benzenedithiolato complexes as models of molybdenum oxidoreductases. *Inorg. Chem.* **1994**, *33*, 209–216. [CrossRef]
9. Davies, E.S.; Beddoes, R.L.; Collison, D.; Dinsmore, A.; Docrat, A.; Joule, J.A.; Wilson, C.R.; Garner, C.D. Synthesis of oxomolybdenum bis(dithiolene) complexes related to the cofactor of the oxomolybdoenzymes. *J. Chem. Soc. Dalton Trans.* **1997**, 3985–3995. [CrossRef]
10. Donahue, J.P.; Goldsmith, C.R.; Nadiminti, U.; Holm, R.H. Synthesis, Structures, and Reactivity of Bis(dithiolene)molybdenum(IV,VI) Complexes Related to the Active Sites of Molybdoenzymes. *J. Am. Chem. Soc.* **1998**, *120*, 12869–12881. [CrossRef]
11. Holm, R.H.; Solomon, E.I.; Majumdar, A.; Tenderholt, A. Comparative molecular chemistry of molybdenum and tungsten and its relation to hydroxylase and oxotransferase enzymes. *Coord. Chem. Rev.* **2011**, *255*, 993–1015. [CrossRef]
12. Periyasamy, G.; Burton, N.A.; Hillier, I.H.; Vincent, M.A.; Disley, H.; McMaster, J.; Garner, C.D. The dithiolene ligand—Innocent or 'non-innocent'? A theoretical and experimental study of some cobalt-dithiolene complexes. *Faraday Discuss.* **2007**, *135*, 469–488. [CrossRef]
13. Adams, H.; Morris, M.J.; Robertson, C.C.; Tunnicliffe, H.C.I. Synthesis of Mono- and Diiron Dithiolene Complexes as Hydrogenase Models by Dithiolene Transfer Reactions, Including the Crystal Structure of $[\{Ni(S_2C_2Ph_2)\}_6]$. *Organometallics* **2019**, *38*, 665–676. [CrossRef]
14. Maroney, M.J.; Ciurli, S. Nonredox Nickel Enzymes. *Chem. Rev.* **2014**, *114*, 4206–4228. [CrossRef]
15. Can, M.; Armstrong, F.A.; Ragsdale, S.W. Structure, Function, and Mechanism of the Nickel Metalloenzymes, CO Dehydrogenase, and Acetyl-CoA Synthase. *Chem. Rev.* **2014**, *114*, 4149–4174. [CrossRef]
16. Lubitz, W.; Ogata, H.; Rüdiger, O.; Reijerse, E. Hydrogenases. *Chem. Rev.* **2014**, *114*, 4081–4148. [CrossRef]
17. Van Gastel, M.; Shaw, J.L.; Blake, A.J.; Flores, M.; Schröder, M.; McMaster, J.; Lubitz, W. Electronic Structure of a Binuclear Nickel Complex of Relevance to [NiFe] Hydrogenase. *Inorg. Chem.* **2008**, *47*, 11688–11697. [CrossRef]
18. Choudhury, S.B.; Pressler, M.A.; Mirza, S.A.; Day, R.O.; Maroney, M.J. Structure and Redox Chemistry of Analogous Nickel Thiolato and Selenolato Complexes: Implications for the Nickel Sites in Hydrogenases. *Inorg. Chem.* **1994**, *33*, 4831–4839. [CrossRef]
19. Mondragón, A.; Flores-Alamo, M.; Martínez-Alanis, P.R.; Aullón, G.; Ugalde-Saldívar, V.M.; Castillo, I. Electrocatalytic Proton Reduction by Dimeric Nickel Complex of a Sterically Demanding Pincer-type NS2 Aminobis(thiophenolate) Ligand. *Inorg. Chem.* **2015**, *54*, 619–627. [CrossRef]
20. Song, L.-C.; Lu, Y.; Cao, M.; Yang, X.-Y. Reactions of dinuclear Ni2 complexes [Ni(RNPyS4)]2 (RNPyS4 = 2,6-bis(2-mercaptophenylthiomethyl)-4-R-pyridine) with Fe(CO)3(BDA) (BDA = benzylidene acetone) leading to heterodinuclear NiFe and mononuclear Fe complexes related to the active sites of [NiFe]- and [Fe]-hydrogenases. *RSC Adv.* **2016**, *6*, 39225–39233.
21. Schrauzer, G.N.; Mayweg, V.P.; Heinrich, W. Coordination Compounds with Delocalized Ground States. α-Dithiodiketone-Substituted Group VI Metal Carbonyls and Related Compounds. *J. Am. Chem. Soc.* **1966**, *88*, 5174–5179. [CrossRef]
22. Schrauzer, G.N. Coordination compounds with delocalized ground states. Transition metal derivatives of dithiodiketones and ethylene-1,2-dithiolates (metal dithienes). *Acc. Chem. Res.* **1969**, *2*, 72–80. [CrossRef]
23. Lim, B.S.; Donahue, J.P.; Holm, R.H. Synthesis and Structures of Bis(dithiolene)molybdenum Complexes Related to the Active Sites of the DMSO Reductase Enzyme Family. *Inorg. Chem.* **2000**, *39*, 263–273. [CrossRef] [PubMed]

24. Obanda, A.; Martinez, K.; Schmehl, R.H.; Mague, J.T.; Rubtsov, I.V.; MacMillan, S.N.; Lancaster, K.M.; Sproules, S.; Donahue, J.P. Expanding the Scope of Ligand Substitution from [M($S_2C_2Ph_2$] (M = Ni^{2+}, Pd^{2+}, Pt^{2+}) To Afford New Heteroleptic Dithiolene Complexes. *Inorg. Chem.* **2017**, *56*, 10257–10267. [CrossRef] [PubMed]
25. Goddard, C.A.; Holm, R.H. Synthesis and Reactivity Aspects of the Bis(dithiolene) Chalcogenide Series $[WIVQ(S_2C_2R_2)2]^{2-}$ (Q = O, S, Se). *Inorg. Chem.* **1999**, *38*, 5389–5398. [CrossRef]
26. Lim, B.S.; Fomitchev, D.V.; Holm, R.H. Nickel Dithiolenes Revisited: Structures and Electron Distribution from Density Functional Theory for the Three-Member Electron-Transfer Series $[Ni(S_2C_2Me_2)_2]^{0,1-,2-}$. *Inorg. Chem.* **2001**, *40*, 4257–4262. [CrossRef]
27. Ghosh, A.C.; Schulzke, C. Selectively detecting Hg^{2+}—A "mercury quick test" with bis-(coumarin–dithiolene) niccolate. *Inorg. Chim. Acta* **2016**, *445*, 149–154. [CrossRef]
28. Kean, C.L.; Pickup, P.G. A low band gap conjugated metallopolymer with nickel bis(dithiolene) crosslinks. *Chem. Commun.* **2001**, 815–816. [CrossRef]
29. Papavassiliou, G.C.; Anyfantis, G.C.; Mousdis, G.A. Neutral Metal 1,2-Dithiolenes: Preparations, Properties and Possible Applications of Unsymmetrical in Comparison to the Symmetrical. *Crystals* **2012**, *2*, 762–811. [CrossRef]
30. Anyfantis, G.C.; Papavassiliou, G.C.; Assimomytis, N.; Terzis, A.; Psycharis, V.; Raptopoulou, C.P.; Kyritsis, P.; Thoma, V.; Koutselas, I.B. Some unsymmetrical nickel 1,2-dithiolene complexes as candidate materials for optics and electronics. *Solid State Sci.* **2008**, *10*, 1729–1733. [CrossRef]
31. Cassoux, P. Molecular (super)conductors derived from bis-dithiolate metal complexes. *Coord. Chem. Rev.* **1999**, *185–186*, 213–232. [CrossRef]
32. Kato, R. Conducting Metal Dithiolene Complexes: Structural and Electronic Properties. *Chem. Rev.* **2004**, *104*, 5319–5346. [CrossRef] [PubMed]
33. Kusamoto, T.; Nishihara, H. Zero-, one- and two-dimensional bis(dithiolato)metal complexes with unique physical and chemical properties. *Coord. Chem. Rev.* **2019**, *380*, 419–439. [CrossRef]
34. Lieffrig, J.; Jeannin, O.; Auban-Senzier, P.; Fourmigué, M. Chiral Conducting Salts of Nickel Dithiolene Complexes. *Inorg. Chem.* **2012**, *51*, 7144–7152. [CrossRef]
35. Neves, A.I.S.; Santos, I.C.; Pereira, L.C.J.; Rovira, C.; Ruiz, E.; Belo, D.; Almeida, M. Ni-2,3-thiophenedithiolate Anions in New Architectures: An In-Line Mixed-Valence Ni Dithiolene (Ni4–S12) Cluster. *Eur. J. Inorg. Chem.* **2011**, *2011*, 4807–4815. [CrossRef]
36. Jeannin, O.; Clérac, R.; Fourmigué, M. Order−Disorder Transition Coupled with Magnetic Bistability in the Ferricinium Salt of a Radical Nickel Dithiolene Complex. *J. Am. Chem. Soc.* **2006**, *128*, 14649–14656. [CrossRef]
37. Deplano, P.; Pilia, L.; Espa, D.; Mercuri, M.L.; Serpe, A. Square-planar d8 metal mixed-ligand dithiolene complexes as second order nonlinear optical chromophores: Structure/property relationship. *Coord. Chem. Rev.* **2010**, *254*, 1434–1447. [CrossRef]
38. Basu, P.; Nigam, A.; Mogesa, B.; Denti, S.; Nemykin, V.N. Synthesis, characterization, spectroscopy, electronic and redox properties of a new nickel dithiolene system. *Inorg. Chim. Acta* **2010**, *363*, 2857–2864. [CrossRef]
39. Alves, H.; Simão, D.; Cordeiro Santos, I.; Gama, V.; Teives Henriques, R.; Novais, H.; Almeida, M. A Series of Transition Metal Bis(dicyanobenzenedithiolate) Complexes [M($dcbdt)_2$] (M = Fe, Co, Ni, Pd, Pt, Cu, Au and Zn). *Eur. J. Inorg. Chem.* **2004**, 1318–1329. [CrossRef]
40. Ghosh, A.C.; Weisz, K.; Schulzke, C. Selective Capture of Ni^{2+} Ions by Naphthalene- and Coumarin-Substituted Dithiolenes. *Eur. J. Inorg. Chem.* **2016**, *2016*, 208–218. [CrossRef]
41. Perochon, R.; Piekara-Sady, L.; Jurga, W.; Clerac, R.; Fourmigue, M. Amphiphilic paramagnetic neutral gold dithiolene complexes. *Dalton Trans.* **2009**, 3052–3061. [CrossRef]
42. Perochon, R.; Poriel, C.; Jeannin, O.; Piekara-Sady, L.; Fourmigué, M. Chiral, Neutral, and Paramagnetic Gold Dithiolene Complexes Derived from Camphorquinone. *Eur. J. Inorg. Chem.* **2009**, *2009*, 5413–5421. [CrossRef]
43. McLauchlan, C.C.; Ibers, J.A. Synthesis and Characterization of the Silver Maleonitrilediselenolates and Silver Maleonitriledithiolates $[K([2.2.2]\text{-cryptand})]_4[Ag_4(Se_2C_2(CN)_2)_4]$, $[Na([2.2.2]\text{-cryptand})]_4[Ag_4(S_2C_2(CN)_2)_4]\cdot 0.33MeCN$, $[NBu_4]_4[Ag_4(S_2C_2(CN)_2)_4]$, $[K([2.2.2]\text{-cryptand})]_3[Ag(Se_2C_2(CN)_2)_2]\cdot 2MeCN$, and $[Na([2.2.2]\text{-cryptand})]_3[Ag(S_2C_2(CN)_2)_2]$. *Inorg. Chem.* **2001**, *40*, 1809–1815.

44. Watanabe, E.; Fujiwara, M.; Yamaura, J.-I.; Kato, R. Synthesis and properties of novel donor-type metal–dithiolene complexes based on 5,6-dihydro-1,4-dioxine-2,3-dithiol (edo) ligand. *J. Mater. Chem.* **2001**, *11*, 2131–2141. [CrossRef]
45. Llusar, R.; Vicent, C. Trinuclear molybdenum cluster sulfides coordinated to dithiolene ligands and their use in the development of molecular conductors. *Coord. Chem. Rev.* **2010**, *254*, 1534–1548. [CrossRef]
46. Castillo, O.; Delgado, E.; Gómez-García, C.J.; Hernández, D.; Hernández, E.; Martín, A.; Martínez, J.I.; Zamora, F. Group 10 Metal Benzene-1,2-dithiolate Derivatives in the Synthesis of Coordination Polymers Containing Potassium Countercations. *Inorg. Chem.* **2017**, *56*, 11810–11818. [CrossRef]
47. Nicholson, J.R.; Christou, G.; Huffman, J.C.; Folting, K. The synthesis, structure and spectroscopic properties of the di- and tri-nuclear Ni(II) thiolate complexes. *Polyhedron* **1987**, *6*, 863–870. [CrossRef]
48. Breitzer, J.G.; Rauchfuss, T.B. Studies on α-$C_3S_5^{2-}$ ($dmit^{2-}$) and its dinuclear Ni(II) complex: Spectroscopic and structural characterization. *Polyhedron* **2000**, *19*, 1283–1291. [CrossRef]
49. Sheng, T.; Zhang, W.; Gao, X.; Lin, P. Two new nickel-dmit-based molecular conductors based on heteroleptic polymetallic complexes: Synthesis, structures and electrical properties. *Chem. Commun.* **1998**, 263–264. [CrossRef]
50. Ahmadi, M.; Fischer, C.; Ghosh, A.C.; Schulzke, C. An Asymmetrically Substituted Aliphatic Bis-Dithiolene Mono-Oxido Molybdenum(IV) Complex With Ester and Alcohol Functions as Structural and Functional Active Site Model of Molybdoenzymes. *Front. Chem.* **2019**, *7*, 486. [CrossRef]
51. Chrysochos, N.; Ahmadi, M.; Wahlefeld, S.; Rippers, Y.; Zebger, I.; Mroginski, M.A.; Schulzke, C. Comparison of molybdenum and rhenium oxo bis-pyrazine-dithiolene complexes—In search of an alternative metal centre for molybdenum cofactor models. *Dalton Trans.* **2019**, *48*, 2701–2714. [CrossRef]
52. Ghosh, A.C.; Samuel, P.P.; Schulzke, C. Synthesis, characterization and oxygen atom transfer reactivity of a pair of Mo(IV)O− and Mo(VI)O2− enedithiolate complexes—A look at both ends of the catalytic transformation. *Dalton Trans.* **2017**, *46*, 7523–7533. [CrossRef]
53. Holleman, A.; Wiberg, N.; Krieger-Hauwede, M. *Anorganische Chemie Band1: Grundlagen und Hauptgruppenelemente*, 103th ed.; Walter de Gruyter: Berlin, Germany; Boston, MA, USA, 2017; Volume 1.
54. Eisenberg, R.; Gray, H.B. Noninnocence in Metal Complexes: A Dithiolene Dawn. *Inorg. Chem.* **2011**, *50*, 9741–9751. [CrossRef]
55. Williams, R.; Billig, E.; Waters, J.H.; Gray, H.B. The Toluenedithiolate and Maleonitriledithiolate Square-Matrix Systems. *J. Am. Chem. Soc.* **1966**, *88*, 43–50. [CrossRef]
56. Yang, J.; Enemark, J.H.; Kirk, M.L. Metal–Dithiolene Bonding Contributions to Pyranopterin Molybdenum Enzyme Reactivity. *Inorganics* **2020**, *8*, 19. [CrossRef]
57. Volbeda, A.; Martin, L.; Cavazza, C.; Matho, M.; Faber, B.W.; Roseboom, W.; Albracht, S.P.J.; Garcin, E.; Rousset, M.; Fontecilla-Camps, J.C. Structural differences between the ready and unready oxidized states of [NiFe] hydrogenases. *J. Biol. Inorg. Chem.* **2005**, *10*, 239–249. [CrossRef]
58. Higuchi, Y.; Yagi, T.; Yasuoka, N. Unusual ligand structure in Ni–Fe active center and an additional Mg site in hydrogenase revealed by high resolution X-ray structure analysis. *Structure* **1997**, *5*, 1671–1680. [CrossRef]
59. Higuchi, Y.; Ogata, H.; Miki, K.; Yasuoka, N.; Yagi, T. Removal of the bridging ligand atom at the Ni–Fe active site of [NiFe] hydrogenase upon reduction with H2, as revealed by X-ray structure analysis at 1.4 Å resolution. *Structure* **1999**, *7*, 549–556. [CrossRef]
60. Ogata, H.; Kellers, P.; Lubitz, W. The Crystal Structure of the [NiFe] Hydrogenase from the Photosynthetic Bacterium Allochromatium vinosum: Characterization of the Oxidized Enzyme (Ni-A State). *J. Mol. Biol.* **2010**, *402*, 428–444. [CrossRef]
61. Marques, M.C.; Tapia, C.; Gutiérrez-Sanz, O.; Ramos, A.R.; Keller, K.L.; Wall, J.D.; De Lacey, A.L.; Matias, P.M.; Pereira, I.A.C. The direct role of selenocysteine in [NiFeSe] hydrogenase maturation and catalysis. *Nat. Chem. Biol.* **2017**, *13*, 544–550. [CrossRef]
62. Volbeda, A.; Charon, M.-H.; Piras, C.; Hatchikian, E.C.; Frey, M.; Fontecilla-Camps, J.C. Crystal structure of the nickel–iron hydrogenase from Desulfovibrio gigas. *Nature* **1995**, *373*, 580–587. [CrossRef]
63. Moubarak, S.; Elghobashi-Meinhardt, N.; Tombolelli, D.; Mroginski, M.A. Probing the Structure of [NiFeSe] Hydrogenase with QM/MM Computations. *Appl. Sci.* **2020**, *10*, 781. [CrossRef]
64. Schlaepfer, C.W.; Nakamoto, K. Infrared spectra and normal-coordinate analysis of 1,2-dithiolate complexes with nickel. *Inorg. Chem.* **1975**, *14*, 1338–1344. [CrossRef]

65. Bui, T.-T.; Thiebaut, O.; Grelet, E.; Achard, M.-F.; Garreau-de Bonneval, B.; Moineau-Chane Ching, K.I. Discotic Nickel Bis(dithiolene) Complexes—Synthesis, Optoelectrochemical and Mesomorphic Properties. *Eur. J. Inorg. Chem.* **2011**, *2011*, 2663–2676. [CrossRef]
66. Kirk, M.L.; McNaughton, R.L.; Helton, M.E. The Electronic Structure and Spectroscopy of Metallo-Dithiolene Complexes. In *Dithiolene Chemistry*; Stiefel, E.I., Ed.; John Wiley & Sons, Inc.: Hoboken, NJ, USA, 2004; Volume 52, pp. 111–212.
67. Ray, K.; Weyhermüller, T.; Neese, F.; Wieghardt, K. Electronic Structure of Square Planar Bis(benzene-1,2-dithiolato)metal Complexes [M(L)2]z (z = 2−, 1−, 0; M = Ni, Pd, Pt, Cu, Au): An Experimental, Density Functional, and Correlated ab Initio Study. *Inorg. Chem.* **2005**, *44*, 5345–5360. [CrossRef]
68. Izutsu, K. Potentiometry in Nonaqueous Solutions. In *Electrochemistry in Nonaqueous Solutions*; Wiley-VCH Verlag GmbH & Co. KGaA: Weinheim, Germany, 2009; Chapter 6; pp. 171–208. [CrossRef]
69. Evans, D.F. 400. The determination of the paramagnetic susceptibility of substances in solution by nuclear magnetic resonance. *J. Chem. Soc.* **1959**, 2003–2005. [CrossRef]
70. Evans, D.F.; James, T.A. Variable-temperature magnetic-susceptibility measurements of spin equilibria for iron(III) dithiocarbamates in solution. *J. Chem. Soc. Dalton Trans.* **1979**, 723–726. [CrossRef]
71. Sheldrick, G. SHELXT—Integrated space-group and crystal-structure determination. *Acta Crsyt. A* **2015**, *71*, 3–8. [CrossRef]
72. Sheldrick, G. Crystal structure refinement with SHELXL. *Acta Cryst. C* **2015**, *71*, 3–8. [CrossRef]
73. Farrugia, L. WinGX and ORTEP for Windows: An update. *J. Appl. Crystallogr.* **2012**, *45*, 849–854. [CrossRef]
74. Ahmadi, M. Phosphate Substituted Dithiolene Complexes as Models for the Active Site of Molybdenum Dependent Oxidoreductases. Universität Greifswald, Greifswald, Germany, 2019. Available online: https://epub.ub.uni-greifswald.de/frontdoor/index/index/start/1/rows/10/sortfield/score/sortorder/desc/searchtype/simple/query/Mohsen+Ahmadi/docId/3279 (accessed on 1 March 2020).